J. Fluid Mech. (2001), *vol.* 445, *pp.* 187–206.
DOI: 10.1017/S0022112001005584 Printed in the United Kingdom

The Fanno model for turbulent compressible flow

By H. OCKENDON[1], J. R. OCKENDON[1] AND S. A. E. G. FALLE[2]

[1]OCIAM, Mathematical Institute, Oxford University, 24–29 St Giles', Oxford OX1 3LB, UK
[2]Department of Applied Mathematics, University of Leeds, Leeds LS2 9JT, UK

(Received 10 May 1999 and in revised form 8 May 2001)

The paper considers the derivation and properties of the Fanno model for nearly unidirectional turbulent flow of gas in a tube. The model is relevant to many industrial processes. Approximate solutions are derived and numerically validated for evolving flows of initially small amplitude, and these solutions reveal the prevalence of localized large-time behaviour, which is in contrast to inviscid acoustic theory. The properties of large-amplitude travelling waves are summarized, which are also surprising when compared to those of inviscid theory.

1. Introduction

The classical theory of quasi-one-dimensional inviscid flow of a perfect gas in a tube, as expounded in Liepmann & Roshko (1957), cannot be applied to situations where the flow is turbulent and where the tube is long enough for wall drag to be important. One industrial situation where this is the case arises in the air-jet spinning of polymer filaments (see European Study Group 1997), where typically the tube (in fact a two-dimensional channel) has aspect ratio 10^{-3}. On a smaller scale the inlets to pressure transducers sometimes have similar geometries (Jones *et al.* 1993) and larger scale examples are those of a high-speed train or pneumatic-tube vehicle travelling through a long tunnel (Ozawa & Maeda 1988; Wright & White 1974). In such configurations, a more realistic model than that of inviscid flow is the Fanno flow model (Knight 1998; Landau & Lifschitz 1959; Shapiro 1953), which includes a drag term in the momentum balance while leaving the equations of mass and energy conservation unaltered.

The Fanno model has received little mathematical attention, and the principal objective of this paper is to describe the underlying modelling assumptions, which we do in § 2, and to make some predictions about travelling and evolving waves, which we do in §§ 3, 4. The mathematical theory will never be as complete as it is for inviscid flow because, although the Fanno model comprises a hyperbolic system of partial differential equations, it does not possess any Riemann invariants. Hence analytical progress can only be made for flows that are either travelling waves or are of small amplitude.

We will frame our description of Fanno flow on the lines usually adopted when a conventional shear viscosity is used to model dissipation. In that theory, the dissipation is strongest where the velocity gradient is greatest; this is particularly true near shock waves, which, when they are weak, are modelled by Burgers equation. In Fanno flow,

however, the wall drag damps flows over large times and distances but has relatively little local effect on shock waves.

2. The Fanno model

The Fanno model for mass, momentum and energy conservation of a quasi-one-dimensional turbulent gas flow in a tube of area $S(x)$ is derived on physical grounds for steady flow in Wright & White (1974), Knight (1998), Landau & Lifschitz (1959), Shapiro (1953). The unsteady form of the equations is

$$\frac{\partial}{\partial t}(\rho S) + \frac{\partial}{\partial x}(\rho u S) = 0, \tag{1}$$

$$\frac{\partial}{\partial t}(\rho u S) + \frac{\partial}{\partial x}(\rho u^2 S) + S\frac{\partial p}{\partial x} = -d\rho f u|u|, \tag{2}$$

$$\frac{\partial}{\partial t}(\rho S(e + \tfrac{1}{2}u^2)) + \frac{\partial}{\partial x}(\rho u S(e + \tfrac{1}{2}u^2)) + \frac{\partial}{\partial x}(puS) = 0, \tag{3}$$

where the gas density, pressure, velocity and internal energy are ρ, p, u, e; f is a positive constant representing the wall drag, d is the perimeter of the tube and the tube is aligned with the x-axis. Only the right-hand side of the momentum equation differs from the classical inviscid model, and hence there appears to be a discrepancy, because dissipation is neglected in the energy equation.

This model can be heuristically validated if we are prepared to start from the following model for the mean turbulent velocity (u^*, v^*), pressure p^* and density ρ^* in a nearly unidirectional two-dimensional flow in a channel $-\frac{1}{2}S(x) < y < \frac{1}{2}S(x)$ whose length is much greater than its typical breadth, so that $\partial/\partial x \ll \partial/\partial y$:

$$\frac{\partial \rho^*}{\partial t} + \frac{\partial}{\partial x}(\rho^* u^*) + \frac{\partial}{\partial y}(\rho^* v^*) = 0, \tag{4}$$

$$\frac{\partial}{\partial t}(\rho^* u^*) + \frac{\partial}{\partial x}(\rho^* u^{*2}) + \frac{\partial}{\partial y}(\rho^* u^* v^*) + \frac{\partial p^*}{\partial x} = \frac{\partial \tau^*}{\partial y}, \tag{5}$$

$$\frac{\partial}{\partial t}(\rho^* E^*) + \frac{\partial}{\partial x}(\rho^* u^* E^*) + \frac{\partial}{\partial y}(\rho^* v^* E^*) + \frac{\partial}{\partial x}(u^* p^*) + \frac{\partial}{\partial y}(p^* v^*) = \frac{\partial}{\partial y}(u^* \tau^*). \tag{6}$$

Here we have denoted the dominant stress component by τ^* and set

$$E^* = \frac{p^*}{(\gamma - 1)\rho^*} + \tfrac{1}{2}u^{*2}$$

where γ is the ratio of specific heats. We have also put $d = 1$ for two-dimensional flow and assumed conduction is negligible.

The two key assumptions of the Fanno model are that

(i) τ^* changes rapidly from a small value outside the boundary layer to τ_w at the wall, so that the right-hand side of (5) is effectively a delta function of strength τ_w at each wall;

(ii) the flow is almost plug flow so that, except for the right-hand sides of (5), (6), all the terms in these equations can be considered as being independent of y when averaging across the tube.

Then, integrating with respect to y from $-S/2$ to $S/2$, using the no-slip condition

and setting $\int_{-S/2}^{S/2} u^* \, \mathrm{d}y = Su$ etc., we obtain (1)–(3) except that the right-hand side of (2) is $2\tau_w$. The final ingredient for the Fanno model is the empirical result that $\tau_w = -\frac{1}{2} f \rho u |u|$ where $f = O(10^{-3})$ (see Knight 1998): this formula is similar to wall friction laws used in hydraulics and it can be deduced by averaging turbulent boundary layer models such as the Cebici–Smith model (Hague *et al.* 1992).

It is convenient to non-dimensionalize these equations by scaling x with a length L much longer than a typical channel width S_0, S with S_0, u and ρ with typical initial or boundary values u_0, ρ_0, and t with L/u_0. We also scale $p - p_0$ with $\rho_0 u_0^2$, where p_0 is a reference value of p, which may seem unnecessarily complicated at this stage but it helps our subsequent investigation into the effects of changing u_0 and p_0 independently.

It is easy to see that if we take $L = S_0/f$, the factor f vanishes from the model. Thus this length scale emerges as the minimum channel length over which the effect of wall friction enters the model to lowest order. Finally, the non-dimensional model, which will form the basis for our analysis, is

$$\frac{\partial}{\partial t}(\rho S) + \frac{\partial}{\partial x}(\rho u S) = 0, \tag{7}$$

$$S\left(\frac{\partial u}{\partial t} + u\frac{\partial u}{\partial x} + \frac{1}{\rho}\frac{\partial p}{\partial x}\right) = -u|u|, \tag{8}$$

$$\frac{\mathrm{d}}{\mathrm{d}t}\left(\frac{p}{(\gamma-1)\rho} + \tfrac{1}{2}u^2\right) - \frac{1}{\rho^2}\left(\frac{1}{(\gamma-1)M_0^2} + p\right)\frac{\mathrm{d}\rho}{\mathrm{d}t} + \frac{u}{\rho}\frac{\partial p}{\partial x} = 0, \tag{9}$$

where

$$\frac{\mathrm{d}}{\mathrm{d}t} = \frac{\partial}{\partial t} + u\frac{\partial}{\partial x} \quad \text{and} \quad M_0^2 = \frac{u_0^2 \rho_0}{\gamma p_0}.$$

The unconventional pressure scaling has resulted in the irritating explicit appearance of this reference Mach number.

The model for flow in a tube would be similar, with S denoting the dimensionless cross-sectional area and the perimeter of this area appearing as a factor on the right-hand side of (8).

As in inviscid flow, system (7)–(9) is hyperbolic with characteristics

$$\frac{\mathrm{d}x}{\mathrm{d}t} = u \pm a \quad \text{and} \quad \frac{\mathrm{d}x}{\mathrm{d}t} = u,$$

where $a^2 = (\gamma p/\rho) + (1/M_0^2\rho)$. However there are no Riemann invariants. Indeed, since (7) and (8) can be used to write (9) as

$$\rho^\gamma \frac{\mathrm{d}}{\mathrm{d}t}\left\{\left(p + \frac{1}{\gamma M_0^2}\right)\rho^{-\gamma}\right\} = \frac{(\gamma-1)\rho u^2 |u|}{S}, \tag{10}$$

entropy is not conserved on a particle path. On the other hand, shocks moving with speed V are possible in which the usual Rankine–Hugoniot conditions hold, so that

$$V = \frac{[\rho u]}{[\rho]} = \frac{[p + \rho u^2]}{[\rho u]} = \frac{[\rho u(h + \frac{1}{2}u^2)]}{[\rho(e + \frac{1}{2}u^2)]}, \tag{11}$$

where

$$h = \frac{\gamma p}{(\gamma-1)\rho} + \frac{1}{(\gamma-1)M_0^2\rho}$$

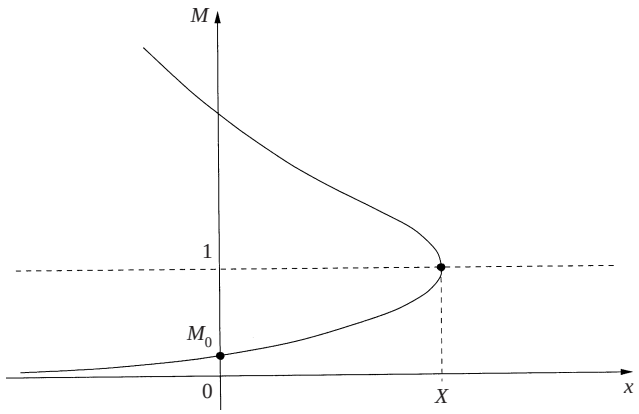

FIGURE 1. Solution of (15) for constant S.

and the dimensionless internal energy is $e = h/\gamma$; uniqueness is expected as long as expansion shocks are forbidden. Note from (8) that wall drag damps the motion both as time increases and as we move in the direction of the flow. For example, when the flow is spatially constant, ρ remains fixed but u decays as $O(t^{-1})$ and p increases to its ultimate value from which it differs by $O(t^{-2})$ as $t \to \infty$.

As described in Wright & White (1974), quasi-one-dimensional steady nozzle flow is described by the ordinary differential equations

$$\frac{\mathrm{d}}{\mathrm{d}x}(\rho u S) = 0, \tag{12}$$

$$\rho u \frac{\mathrm{d}u}{\mathrm{d}x} + \frac{\mathrm{d}p}{\mathrm{d}x} = -\rho u|u|/S, \tag{13}$$

$$\frac{\mathrm{d}}{\mathrm{d}x}[\rho u S(h + \tfrac{1}{2}u^2)] = 0, \tag{14}$$

which can be reduced to

$$\frac{\mathrm{d}M}{M}\frac{(1 - M^2)}{1 + \frac{1}{2}(\gamma - 1)M^2} + \frac{\mathrm{d}S}{S} = \frac{\gamma M|M|\,\mathrm{d}x}{S}, \tag{15}$$

where the Mach number is $M = u/a$. Thus, as far as the Mach number is concerned, the frictional effects are similar to those resulting from a converging channel for which $\mathrm{d}S/S$ is negative. However, it should be remembered that friction always increases the entropy, whereas the shock-free flow of an inviscid fluid through a channel of varying cross-section is isentropic.

An immediate consequence of this analysis is to enable us to see that wall drag causes the phenomenon of choking to occur even in a constant-area nozzle as soon as the pressure drop is large enough for the exit Mach number to reach unity (figure 1). Any further decrease in exit pressure will leave the flow in the nozzle unaffected, with a shock being expelled from the end of the tube. This phenomenon clearly has important implications for the design of industrial nozzles such as those used in air-jet spinning.

We now turn to two aspects of the Fanno model that have not been addressed in the literature, namely the evolution of small-amplitude waves, and the possibility of large-amplitude travelling waves. In both cases we consider a channel of constant width and set $S = 1$.

3. Small Mach number waves

The most convenient form of equations (7)–(9) from which to start is

$$\frac{\partial \rho}{\partial t} + \frac{\partial}{\partial x}(\rho u) = 0, \tag{16}$$

$$\frac{\partial u}{\partial t} + u\frac{\partial u}{\partial x} + \frac{1}{\rho}\frac{\partial p}{\partial x} = -u|u|, \tag{17}$$

$$\frac{\partial p}{\partial t} + u\frac{\partial p}{\partial x} + \left(\frac{1}{M_0^2} + \gamma p\right)\frac{\partial u}{\partial x} = (\gamma - 1)\rho u^2|u|, \tag{18}$$

and the Rankine–Hugoniot relations for a shock moving with non-dimensional speed V are

$$[\rho(V-u)] = 0, \quad [p + \rho(V-u)^2] = 0 \quad \text{and} \quad [h + \tfrac{1}{2}(u-V)^2] = 0.$$

We now study the evolution of small-amplitude waves in two configurations; in each case the gas is initially at rest with pressure p_0 and density ρ_0 in a semi-infinite tube $x > 0$. The first problem, which is relevant to transducer design, considers the flow produced in the tube when the pressure at the end $x = 0$ is suddenly changed by an amount small compared to p_0; the second problem, which may give insight into the air flow generated by high-speed trains in tunnels (Ozawa & Maeda 1988), is the classical problem in which a piston $x = 0$ is moved impulsively with a constant velocity which is small compared to a_0, the speed of sound in the undisturbed gas.

We note that the Fanno model (16)–(18) was derived for dimensional times of $O(S_0/fu_0)$ and lengths of $O(S_0/f)$ over which the wall friction has an $O(1)$ effect. In each of the two problems now considered the Mach number will be everywhere small and frictional effects will be unimportant until the flow has had sufficient time for these scalings to be appropriate. Thus the initial motion is exactly that of a small disturbance in inviscid gas flow and the flow implications of the viscous drag terms will only become apparent for later times. In fact, we will discover that the full Fanno model (16)–(18) will never be needed in either of these problems.

3.1. *Pressure waves*

We suppose that the pressure at the orifice $x = 0$ is changed from p_0 to $p_0(1 + \gamma\epsilon)$ at $t = 0$ where $\epsilon > 0$ and we can therefore assume that $u > 0$ throughout the flow. This boundary condition implies that, for small times, the velocity of the gas will be of order ϵa_0 where $a_0 = \sqrt{\gamma p_0/\rho_0}$ is the speed of sound in the undisturbed gas. We define $u_0 = \epsilon a_0$ and then there is no need to rescale the dimensionless velocity u but, because the dimensional pressure variations are of $O(\epsilon p_0)$, we do need to rescale

$$p = \frac{1}{\epsilon}\tilde{p}$$

and

$$\rho = 1 + \epsilon\tilde{p}.$$

Putting these scalings into (16)–(18) leads, at lowest order, to

$$\frac{\partial u}{\partial x} = 0 \quad \text{and} \quad \frac{\partial \tilde{p}}{\partial x} = 0, \tag{19}$$

with $\tilde{p} = 1$ at $x = 0$ and so the solution is just $\tilde{p} = 1$. The failure of $\tilde{p}$ to satisfy its initial condition of zero is because our scaling has not taken account of the acoustic

wave which propagates ahead of the Fanno flow region. To remedy this, we must look at shorter time scales than those relevant to Fanno flow and so we write $t = \epsilon\tau$.

Equations (16)–(18) then become

$$\frac{\partial\tilde{\rho}}{\partial\tau} + \frac{\partial u}{\partial x} + \epsilon\frac{\partial}{\partial x}(\tilde{\rho}u) = 0, \tag{20}$$

$$(1+\epsilon\tilde{\rho})\left(\frac{\partial u}{\partial\tau} + \epsilon u\frac{\partial u}{\partial x}\right) + \frac{\partial\tilde{p}}{\partial x} = -\epsilon(1+\epsilon\tilde{\rho})u|u|, \tag{21}$$

$$\frac{\partial\tilde{p}}{\partial\tau} + \frac{\partial u}{\partial x} + \epsilon u\frac{\partial\tilde{p}}{\partial x} + \gamma\epsilon\tilde{p}\frac{\partial u}{\partial x} = \epsilon^2(\gamma-1)(1+\epsilon\tilde{\rho})u^2|u|. \tag{22}$$

In scaled variables, the shock relations for a shock moving into the undisturbed region are

$$\left.\begin{aligned} \tilde{\rho} - u + \epsilon\tilde{\rho}(\tilde{V} - u) = 0, \\ \tilde{p} - u - \epsilon u\tilde{V} = 0, \\ 2\tilde{V} - \tfrac{1}{2}(\gamma+1)u + \epsilon\tilde{V}(\tilde{V} - \tfrac{1}{2}(\gamma+1)u) = 0 \end{aligned}\right\} \tag{23}$$

on $\mathrm{d}x/\mathrm{d}\tau = 1 + \epsilon\tilde{V}$ where $V = (1+\epsilon\tilde{V})/\epsilon$. The initial and boundary conditions are

$$u = \tilde{p} = \tilde{\rho} = 0 \quad \text{when} \quad \tau = 0 \quad \text{for} \quad x > 0, \tag{24}$$

and

$$\tilde{p} = 1 \quad \text{on} \quad x = 0 \quad \text{for} \quad \tau > 0. \tag{25}$$

For times where $\tau = O(1)$, wall drag is negligible and, to lowest order,

$$u = \tilde{p} = \tilde{\rho} = 1 \quad \text{when} \quad 0 < x < \tau(1 + \tfrac{1}{4}(\gamma+1)\epsilon), \tag{26}$$

and the shock speed is given by $\tilde{V} = \frac{1}{4}(\gamma+1)$.

Thereafter we encounter a sequence of time scales and over each one the wall drag has a different effect. It turns out that the two most important regimes are when $\tau = O(\epsilon^{-1})$ and $\tau = O(\epsilon^{-2})$, the region in which (19) holds being subsumed in the former. We will use suffices 1 and 2 to refer to these two time zones.

(i) $\tau = O(\epsilon^{-1})$

It is only over times τ of $O(\epsilon^{-1})$ that wall drag can first affect the lowest-order solution, so we set $\tau = \tau_1/\epsilon$. First we consider the flow near the shock, whose position and strength we study by keeping $x - \tau = X$ of $O(1)$ as $\epsilon \to 0$. From (20)–(22), this gives that

$$\frac{\partial}{\partial X}(u - \tilde{\rho}) + \epsilon\left(\frac{\partial\tilde{\rho}}{\partial\tau_1} + \frac{\partial}{\partial X}(\tilde{\rho}u)\right) = 0, \tag{27}$$

$$\frac{\partial}{\partial X}(-u + \tilde{p}) + \epsilon\left(\frac{\partial u}{\partial\tau_1} + u\frac{\partial u}{\partial X}\right) + \epsilon\tilde{\rho}\left(-\frac{\partial u}{\partial X} + \epsilon\left(\frac{\partial u}{\partial\tau_1} + u\frac{\partial u}{\partial X}\right)\right) + \epsilon(1+\epsilon\tilde{\rho})u^2 = 0, \tag{28}$$

and

$$\frac{\partial}{\partial X}(u - \tilde{p}) + \epsilon\left(\frac{\partial\tilde{p}}{\partial\tau_1} + u\frac{\partial\tilde{p}}{\partial X} + \gamma\tilde{p}\frac{\partial u}{\partial X}\right) - \epsilon^2(\gamma-1)(1+\epsilon\tilde{\rho})u^3 = 0. \tag{29}$$

The calculation is similar to that leading to Burgers equation (see for example Liepmann & Roshko 1957), and it gives that, to lowest order, $u = \tilde{p} = \tilde{\rho}$. The

solvability condition for the second-order terms in the expansions of these variables then gives

$$2\frac{\partial u}{\partial \tau_1} + (1+\gamma)u\frac{\partial u}{\partial X} = -u^2. \tag{30}$$

Now a simple calculation using characteristics, the Rankine–Hugoniot conditions for a weak shock, and the matching condition with (26) as $\tau_1 \to 0$ leads to

$$u = \begin{cases} 2/(2+\tau_1) & \text{if } X < \frac{1}{2}(\gamma+1)\ln(1+\frac{1}{2}\tau_1) \\ 0 & \text{if } X > \frac{1}{2}(\gamma+1)\ln(1+\frac{1}{2}\tau_1). \end{cases} \tag{31}$$

We are now in a position to study the flow between the orifice and the shock. Writing $x_1 = \epsilon x$, the first-order problem in x_1 and τ_1 is

$$\frac{\partial \tilde{p}}{\partial \tau_1} + \frac{\partial u}{\partial x_1} = 0, \tag{32}$$

$$\frac{\partial u}{\partial \tau_1} + \frac{\partial \tilde{p}}{\partial x_1} = -u^2, \tag{33}$$

$$\frac{\partial \tilde{p}}{\partial \tau_1} + \frac{\partial u}{\partial x_1} = 0. \tag{34}$$

Eliminating $\tilde{p}$, we obtain the nonlinear wave equation

$$\frac{\partial^2 u}{\partial \tau_1^2} - \frac{\partial^2 u}{\partial x_1^2} = -2u\frac{\partial u}{\partial \tau_1}, \tag{35}$$

with boundary conditions

$$\tilde{p} = 1 \quad \text{or} \quad \frac{\partial u}{\partial x_1} = 0 \quad \text{on} \quad x_1 = 0, \tag{36}$$

and, to match with (31),

$$u = \tilde{p} = \frac{2}{2+\tau_1} \quad \text{on} \quad x_1 = \tau_1. \tag{37}$$

Although this Goursat problem is well-posed (Garabedian 1964, p. 117) it does not appear to have an explicit analytic solution. However an important feature of the structure of the solution is revealed by noting that we can integrate along the characteristic $x_1 = \tau_1$ where, from (35) and (37),

$$\frac{\mathrm{d}}{\mathrm{d}\tau_1}\left(2\frac{\partial u}{\partial \tau_1} + \frac{2}{(\tau_1+2)^2}\right) + \frac{4}{\tau_1+2}\frac{\partial u}{\partial \tau_1} = 0,$$

and

$$\frac{\mathrm{d}u}{\mathrm{d}\tau_1} = \frac{\partial u}{\partial x_1} + \frac{\partial u}{\partial \tau_1} = -\frac{2}{(2+\tau_1)^2}.$$

Hence on $x_1 = \tau_1$,

$$\frac{\partial u}{\partial \tau_1} = \frac{2\ln(\tau_1+2)+c}{(\tau_1+2)^2},$$

$$\frac{\partial u}{\partial x_1} = \frac{-2\ln(\tau_1+2)-c-2}{(\tau_1+2)^2},$$

where c is a constant that cannot be determined by purely local considerations. From this we can see that not only u but also its first derivatives decay algebraically along the shock. This result suggests that the shock has a negligible role to play in the subsequent evolution. In any case, we can now begin to build up a map of the asymptotic regions in the (x,τ)-plane as in figure 3 below.

(ii) $\tau = O(\epsilon^{-2})$

For larger values of τ, the solution becomes easier to analyse asymptotically. We first observe that (30) remains unchanged if τ_1 is scaled with ϵ^{-n} and u with ϵ^n which suggests that this equation continues to describe the solution when $X = x - \tau = O(1)$ for all time. In particular when $\tau = \epsilon^{-2}\tau_2$, $x = \epsilon^{-2}x_2$ we get

$$u = \frac{2\epsilon}{\tau_2} \quad \text{on} \quad x_2 = \tau_2. \tag{38}$$

Further behind the shock, when τ_2, x_2 are both $O(1)$ we write $u = \epsilon u_2$, $\tilde{p} = \epsilon p_2$ and $\tilde{\rho} = \epsilon\rho_2$ and find that (35) still holds for u_2 as a function of x_2 and τ_2. However, the boundary condition (38) now allows a similarity solution of the form

$$u_2 = \frac{1}{\tau_2}g(\eta), \quad p_2 = \frac{1}{\tau_2}h(\eta),$$

where $\eta = x_2/\tau_2$, $g' = h + \eta h'$, $' = \mathrm{d}/\mathrm{d}\eta$ and

$$(\eta^2 - 1)g'' + 4\eta g' + 2g = 2g(g + \eta g'), \tag{39}$$

with $g(1) = 2$ from (38) and $g \to \infty$ as $\eta \to 0$. This last condition comes from the fact that $\tilde{p} = 1$ on $X = 0$ and so $p_2 \to \infty$ as $x_2 \to 0$.

We can give a heuristic argument that this two-point boundary value problem has a unique solution for g by noting that

(a) as $\eta \to 0$, either g has a regular expansion in which $g \sim \alpha_0 + \eta\alpha_1 + \ldots$ with the constants α_0, α_1 providing a two-parameter family of such solutions, or g is singular with $g \sim 3/\eta^2 + \beta_0 + \ldots$ with the constant β_0 providing a one-parameter family of singular solutions;

(b) as $\eta \to 1$, g has a regular expansion in powers of $\eta - 1$ unless g tends to an integer. In particular if $g \to 2$, $g \sim 2 + 2(\eta - 1)\log(1 - \eta) + \gamma_0(\eta - 1) + \ldots$, with the constant γ_0 providing a one-parameter family of such solutions. Thus it is plausible that β_0 and γ_0 will each be uniquely determined, and a rigorous proof of this conjecture has recently been given by Hastings, McLeod & Troy (2001).

Assuming this to be the case we must now consider how p_2 grows as $\eta \to 0$ in order to enable $\tilde{p}$ to satisfy the boundary condition on $x = 0$. Since $p_2 \sim 3\tau_2^2/x_2^3$, and we require $p_2 = O(\epsilon^{-1})$, we write $x_2 = \epsilon^{1/3}\bar{x}_2$ and $u_2 = \epsilon^{-2/3}\bar{u}_2$, which means that $x = O(\epsilon^{-5/3})$ and $u = O(\epsilon^{1/3})$ respectively. We then have the inner problem

$$\frac{\partial\tilde{p}}{\partial\bar{x}_2} = -\bar{u}_2^2, \tag{40}$$

$$\frac{\partial\tilde{p}}{\partial\tau_2} + \frac{\partial\bar{u}_2}{\partial\bar{x}_2} = 0, \tag{41}$$

with boundary conditions $\tilde{p} = 1$ on $\bar{x}_2 = 0$ and

$$\tilde{p} \sim \frac{3\tau_2^2}{\bar{x}_2^3} \quad \text{as} \quad \bar{x}_2 \to \infty.$$

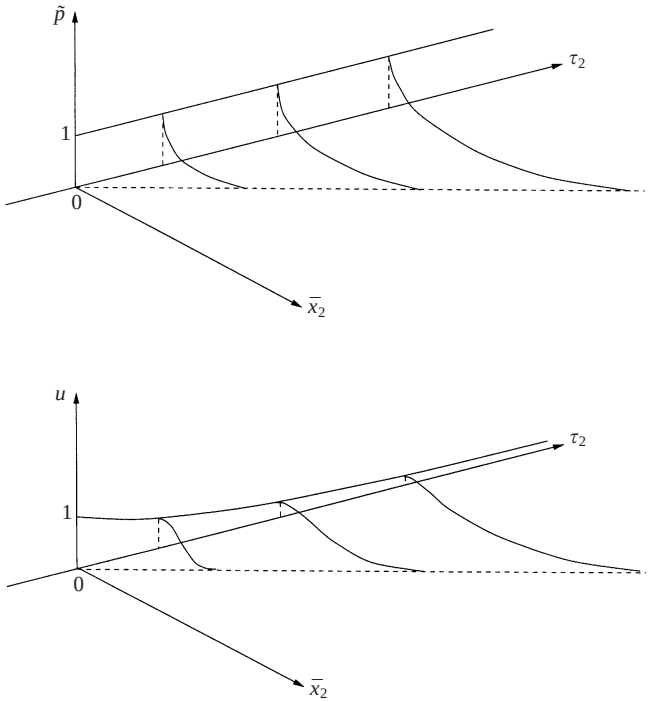

FIGURE 2. Sketch of solution (42) and (43).

Fortunately this parabolic problem has an explicit solution

$$\tilde{p} = 1 - \frac{2}{\pi}\tan^{-1}(\zeta) - \frac{2\zeta}{\pi(1+\zeta^2)}, \tag{42}$$

where $\zeta = (4/9\pi)^{1/3}\,\bar{x}_2/\tau_2^{2/3}$, and the corresponding solution for u is

$$u = \frac{3\epsilon^{1/3}\tau_2}{\bar{x}_2^2 + \left(\frac{9}{4}\pi\tau_2^2\right)^{2/3}}. \tag{43}$$

Summarizing the solution when $\tau = O(\epsilon^{-2})$, we see that when $x = O(\tau)$ both $\tilde{p}$ and u are $O(\epsilon)$ but $\tilde{p}$ grows to $O(1)$ and u to $O(\epsilon^{1/3})$ in a region nearer the orifice where $\epsilon^{1/3}x/\tau^{2/3} = O(1)$ and these solutions are sketched in figure 2.

For larger times, where $\tau \gg O(\epsilon^{-2})$, the same structure persists; the flow becomes increasingly weak when $x = O(\tau)$ but it is still described by the solution of (39) and whenever $\zeta = \epsilon^{1/3}x/\tau^{2/3} = O(1)$, (42) continues to hold. Thus the ultimate effect of the wall drag is to restrict the wave to a region relatively close to the orifice. Thus we can now complete the parameter map of asymptotic solutions as shown in figure 3.

The above predictions have been tested numerically using a second-order Godunov scheme that uses an averaging function to reduce the order in the neighbourhood of discontinuities. The details of the method are given in Falle (1991); see also Terenzi, Mancini & Podenzani (2000). Figure 4 shows a comparison between a numerical solution of equations (20)–(22) and the solution (42) at $\tau = 4518$. The variable plotted is $1 + \gamma\epsilon^2 p$ where $\gamma = 5/3$ and $\epsilon = 0.006$ and good agreement is seen as expected when $\tau \geqslant O(\epsilon^{-2})$.

A very similar scenario describes the flow if the inlet pressure is suddenly reduced

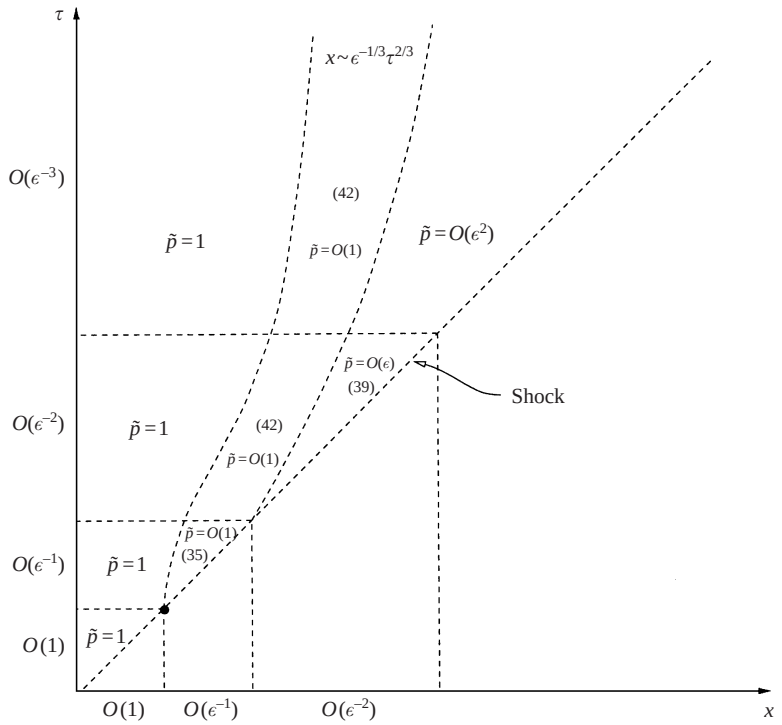

FIGURE 3. Solution of the compressive pressure problem (§ 3.1): regions of the (x, τ)-plane.

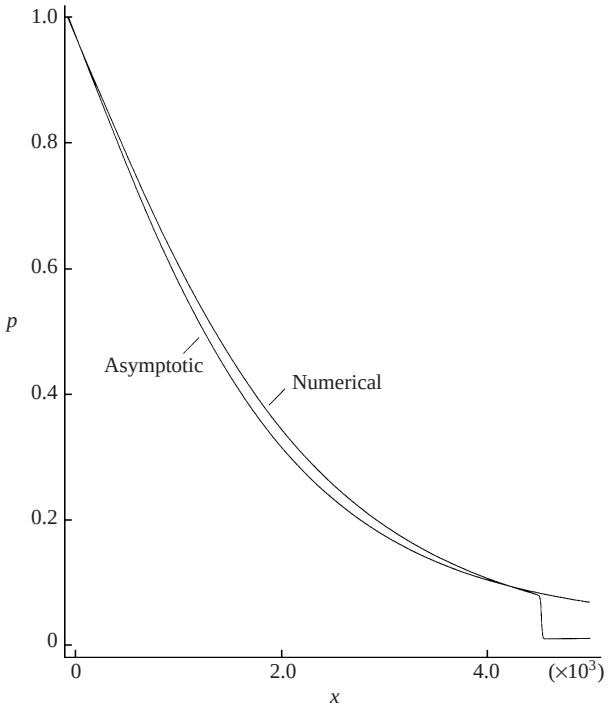

FIGURE 4. Comparison of numerical solution of (20)–(22) with asymptotic solution (42) when $\tau = 4518$, $\epsilon = 0.006$.

by $O(\epsilon)$ at $x = 0$. We may now think of the gas in $x < 0$ (so that u is still always positive) and, by replacing $\tilde{p}$ by $-\tilde{p}$ and x by $-x$, we are led to (39) and (42) exactly as above. The only difference is that what was a shock near $x = \tau$ is now replaced by a weak expansion wave near the characteristic $x = -\tau$ when x and τ are $O(1)$.

3.2. *Piston problem*

We now turn to the more classical problem of gas driven by a piston and here we will find a strong asymmetry between the compression and expansion waves for long time scales. Also our small-Mach-number analysis will reveal regimes of large-amplitude flow, which will motivate a more general study of travelling wave solutions of the Fanno flow equations in § 4.

We consider a piston moved impulsively with constant velocity u_0 where $u_0 \ll a_0$ and again define $\epsilon = u_0/a_0$ as a small parameter. We can then take the same scalings as in § 3.1, and if we immediately proceed to the acoustic scale by writing $t = \epsilon\tau$ we again obtain equations (20)–(22), but in this case the boundary condition is

$$u = 1 \quad \text{on} \quad x = \epsilon\tau.$$

We first consider the compressive wave in $x > 0$.

3.2.1. *Compressive motion*

For x, τ of $O(1)$ the solution (26) still holds. Similarly when x, τ are $O(\epsilon^{-1})$, (30) is still valid near the shock and (35) holds between the piston and the shock with the only difference being that the boundary condition (36) is replaced by

$$u = 1 \quad \text{on} \quad x_1 = 0. \tag{44}$$

When we proceed to $\tau = O(\epsilon^{-2})$, we find that the analysis for $x = O(\epsilon^{-2})$ is unchanged until we reach the scaling described before (40). Now to conform with boundary condition (44) we find we must set $x_2 = \epsilon^{1/2}\hat{x}_2$ (or $x = \epsilon^{-3/2}\hat{x}_2$) which again leads to equations (40) and (41) so that

$$\frac{\partial^2 u}{\partial \hat{x}_2^2} = 2u\frac{\partial u}{\partial \tau_2}, \tag{45}$$

but now the boundary conditions are $u = 1$ on $\hat{x}_2 = 0$ and $u \sim 3\tau_2/\hat{x}_2^2$ as $\hat{x}_2 \to \infty$. Once again we can find a similarity solution, this time of the form

$$u = f(\psi) \quad \text{where} \quad \psi = \frac{\hat{x}_2}{\tau_2^{1/2}}.$$

The equation for f is

$$f'' + \psi f f' = 0, \tag{46}$$

with $f(0) = 1$ and $f \sim 3/\psi^2$ as $\psi \to \infty$. This equation can be simplified by introducing variables $P = \psi^2 f$, $Q = \psi^3 f'$ to obtain

$$\frac{\mathrm{d}Q}{\mathrm{d}P} = \frac{Q(3-P)}{Q+2P}.$$

Consideration of the phase plane (figure 5) shows that there is a unique solution to this problem. It should be noted that $\tilde{p}$ and $\tilde{\rho}$ are of $O(\epsilon^{-1/2})$ here while u remains of $O(1)$ and there is already a stronger localization of the wave near the piston than was the case for the open-ended tube (figure 6).

The piston problem differs further from the open-ended tube problem in that

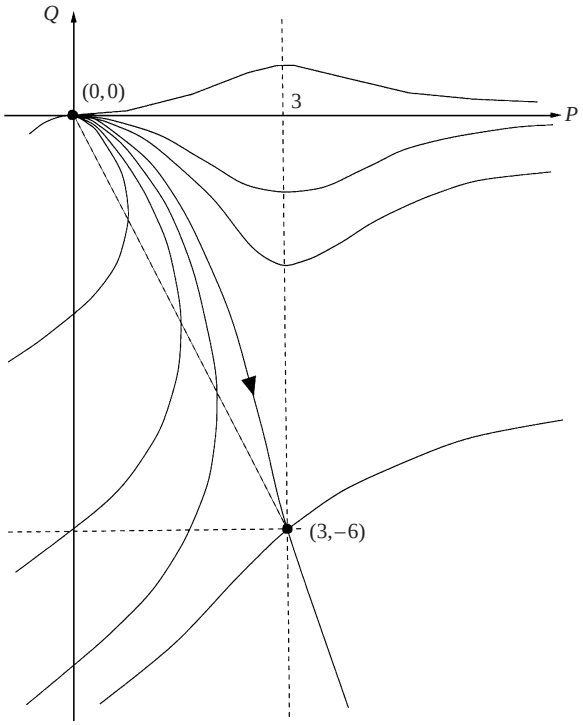

FIGURE 5. The (P, Q) phase plane: $\mathrm{d}Q/\mathrm{d}P = Q(3-P)/(2P+Q)$. The required solution goes from $(0,0)$ to $(3,-6)$.

the solution for $\tau = O(\epsilon^{-2})$ does not persist for longer times. When $\tau = O(\epsilon^{-3})$ the localization is accentuated and the region in which u is $O(1)$ occurs when $x = O(\epsilon^{-2})$ and where $\tilde{p}$ and $\tilde{\rho}$ have now grown to be of $O(\epsilon^{-1})$. Because the pressure perturbations have grown to be as large as the ambient pressure, it is now convenient to set $1 + \epsilon\gamma\tilde{p} = p_3$, $1 + \epsilon\tilde{\rho} = \rho_3$ and $\tau = \epsilon^{-3}\tau_3$, so that

$$\frac{\partial \rho_3}{\partial \tau_3} + \frac{\partial}{\partial x_2}(\rho_3 u) = 0, \tag{47}$$

$$\frac{\partial p_3}{\partial x_2} = -\gamma \rho_3 u^2, \tag{48}$$

$$\frac{\partial p_3}{\partial \tau_3} + \gamma \frac{\partial}{\partial x_2}(p_3 u) = 0, \tag{49}$$

with $u = 1$ on $x_2 = \tau_3$ and $u \to 3\tau_3/x_2^2$ as $\tau_3 \to 0$ and $x_2 \to \infty$. The corresponding limits for p_3 and ρ_3 are given by $\epsilon\tilde{p} \sim \epsilon\tilde{\rho} \to 3\tau_3^2/x_2^3$ as $\tau_3 \to 0$ or $x_2 \to \infty$. The pressure has now built up to such a large value on the piston that the pressure gradient simply balances the friction forces and the inertia terms in (21) are negligible. Although (47)–(49) appear to be almost as hard to analyse as the full problem (20)–(22), their large-time solution is both interesting and simple to describe.

We propose that, for $\tau \gg O(\epsilon^{-3})$, a nearly uniform flow with velocity $u \sim 1$ is set up in the region $\epsilon\tau < x < c\epsilon\tau$, that is between the piston and a wave moving with speed $\epsilon c > 1$, to be determined; ahead of this wave the gas is effectively at rest. The emergence of this flow structure is suggested by writing $x = c\epsilon\tau + \epsilon^{-2}\xi$, so that

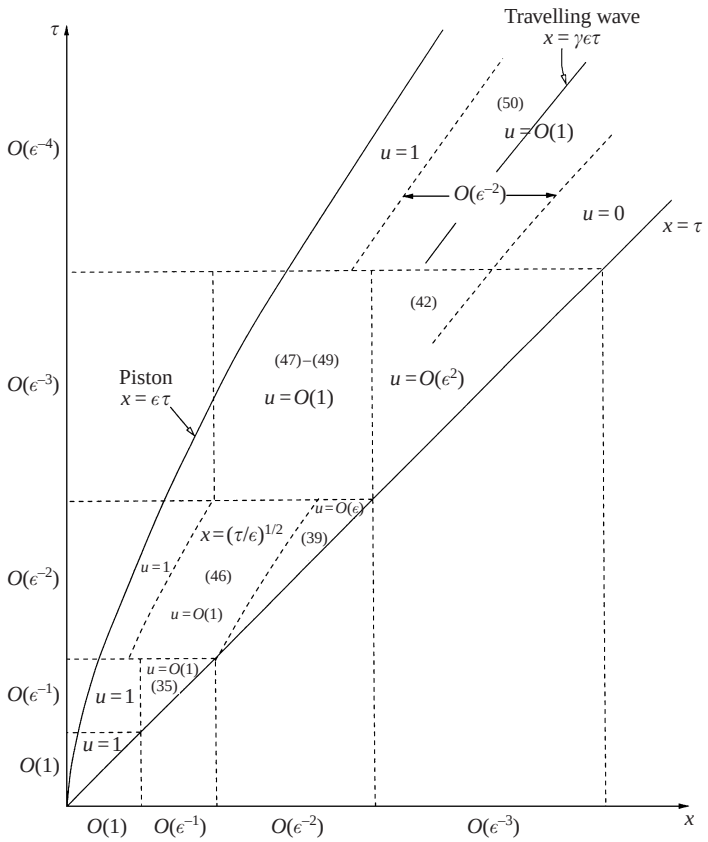

FIGURE 6. Solution of the compressive piston problem (§ 3.2.1): regions of the (x, τ)-plane.

$\xi = x_2 - c\tau_3$; (47)–(49) then imply that

$$\frac{\mathrm{d}u}{\mathrm{d}\xi} = \frac{u^2(\gamma u - c)^2}{u - c},$$

with $u \to 1$ as $\xi \to -\infty$ and $u \to 0$ (with $\rho_3 \to 1$, $p_3 \to 1$) as $\xi \to +\infty$. These conditions can only be satisfied by choosing $c = \gamma$, and then

$$\frac{\mathrm{d}u}{\mathrm{d}\xi} = \frac{-\gamma^2 u^2(1-u)^2}{\gamma - u}; \tag{50}$$

this equation always has a continuous solution, unique apart from a shift in ξ, such that $u \to 0$ as $\xi \to \infty$ and $u \sim 1 + (\gamma - 1)/\gamma^2\xi$ as $\xi \to -\infty$. Moreover $\rho_3 = \gamma/(\gamma - u) \sim \gamma/(\gamma - 1)$ and $p_3 \sim 1/(1-u) \sim -\gamma^2\xi/(\gamma - 1)$ as $\xi \to -\infty$. What has happened is that a wave travelling at precisely γ times the speed of the piston can run just far enough ahead for the pressure and wall drag to balance indefinitely without further change of shape of the wave. In the region between the wave and the piston, u and ρ_3 are approximately 1 and $\gamma/(\gamma - 1)$ respectively and it is easy to see that $p_3 \sim \epsilon^2\gamma^2(\epsilon\gamma\tau - x)/(\gamma - 1)$, the piston pressure attaining the value $\gamma^2\tau_3$. The situation is indicated schematically in figure 6.

In view of the above speculations, it is now even more important to test our predictions numerically than it was for a pressure wave. Since we are using an explicit code for which the time step is limited by the Courant condition, the computation

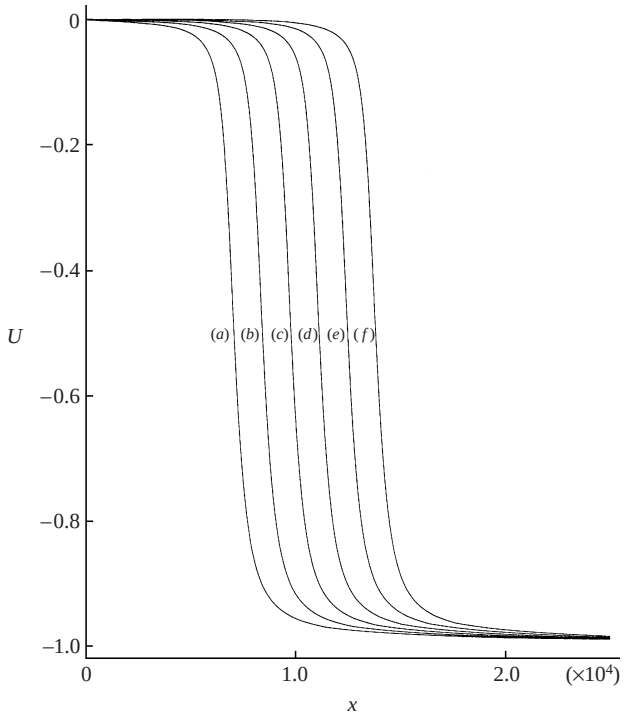

FIGURE 7. Numerical solution of (20)–(22) for piston problem: values of U for $\epsilon = 0.07746$ and (*a*) $\tau = 1.3 \times 10^5$, (*b*) $\tau = 1.55 \times 10^5$, (*c*) $\tau = 1.8 \times 10^5$, (*d*) $\tau = 2.05 \times 10^5$, (*e*) $\tau = 2.3 \times 10^5$, (*f*) $\tau = 2.55 \times 10^5$. Note that the axes shown are measured from the piston.

time required to attain times of $O(\epsilon^{-3})$ becomes extremely large for small values of ϵ. We were, however, able to integrate up to $\tau = O(\epsilon^{-4})$ for $\epsilon = 0.0775$.

The most convenient way to do the numerical calculation is to transform to the piston frame $X = x - \epsilon\tau$ and take $U = u - 1$ so that we impose the conditions $U = 0$ at the piston $X = 0$ and $U = -1$ as $X \to \infty$. From figure 7, which shows the numerical solution for the velocity in the piston frame when $\epsilon = 0.07746$, it can be seen that a travelling wave solution is attained by the time $\tau = O(10^5)$. The speed of the wave in the piston frame is $\mathrm{d}X/\mathrm{d}\tau = 0.056$ which agrees well with the predicted value for $\mathrm{d}X/\mathrm{d}\tau = (\gamma\epsilon) - \epsilon = 0.052$.

As expected, the pressure increases linearly with time at the piston as shown in the plot of p_3 in figure 8. When $\tau = 1.3 \times 10^5$, the numerical solution gives a pressure gradient of -0.023 in comparison with a predicted value of $-\epsilon^2\gamma^2/(\gamma - 1) = -0.025$. In figure 9, the numerical solution for $\tau = 2.55 \times 10^5$ is compared with the travelling wave solution given by (50).

3.2.2. *Expansion waves*

As in the case of the open-ended tube, we can study the structure of the solution to the piston-withdrawal problem by reversing the sign of $x, \tilde{p}$ and $\tilde{\rho}$ and considering gas in the region $x < \epsilon\tau$ driven in the positive x-direction by a piston at $x = t = \epsilon\tau$. For times up to $\tau = O(\epsilon^{-3})$ the scenario is more or less as in § 3.2.1 except that, instead of a shock near $x = \tau$, there is an expansion fan near $x = -\tau$. The variation of u across this fan is of $O(\epsilon^{-1}\tau^{-1})$ and this again becomes insignificant for $\tau > O(\epsilon^{-2})$. However, we see a dramatic contrast with the compressive flow when $\tau_3 \to \infty$. Instead

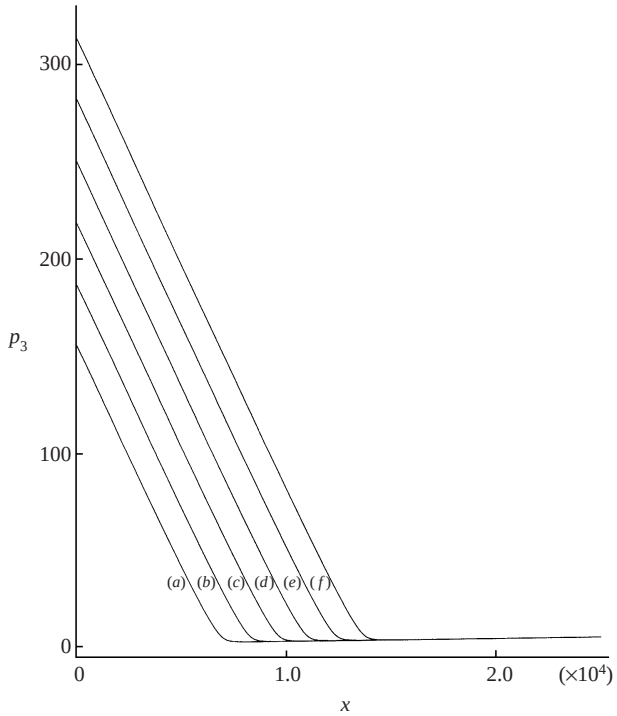

FIGURE 8. Numerical solution of (20)–(22) for piston problem: values of p_3 for $\epsilon = 0.07746$ and the same values of τ as in figure 7.

of a travelling wave emerging near $x = \gamma\varepsilon\tau$, we propose a scenario in which the flow variations are most noticeable in a region relatively close to the initial piston position, with more gradual variations occurring on either side of this region.

To make this specific, suppose $\tau = \epsilon^{-4}\tau_4$. The intractable equations (47)–(49) can be rescaled by setting $x_2 = \epsilon^{-2/3}x_4$, $u = \epsilon^{1/3}u_4$. This means that we are in a region in which $x = O(\epsilon^{-8/3})$, and we retrieve (47)–(49), namely

$$\frac{\partial \rho_3}{\partial \tau_4} + \frac{\partial}{\partial x_4}(\rho_3 u_4) = 0, \tag{51}$$

$$\frac{\partial p_3}{\partial x_4} = -\gamma \rho_3 u_4^2, \tag{52}$$

$$\frac{\partial p_3}{\partial \tau_4} + \gamma \frac{\partial}{\partial x_4}(p_3 u_4) = 0. \tag{53}$$

However, anticipating quiescence as $x_4 \to -\infty$, the boundary conditions are

$$p_3 \sim 1, \quad \rho_3 \sim 1, \quad u_4 \sim 3\tau_4/x_4^2 \quad \text{as} \quad x_4 \to -\infty,$$

and, in order to pave the way for u to be of $O(1)$ near the piston,

$$u_4 \to \infty \quad \text{as} \quad x_4 \to +\infty.$$

Note that the piston is at $x_4 = \epsilon^{-1/3}\tau_4$, and the fact that (51)–(53) are to be solved in $-\infty < x_4 < \infty$ means that we can seek a similarity solution in which

$$p_3 = p_3(\chi), \quad \rho_3 = \rho_3(\chi), \quad u_4 = \tau_4^{-1/3}\bar{u}_4(\chi)$$

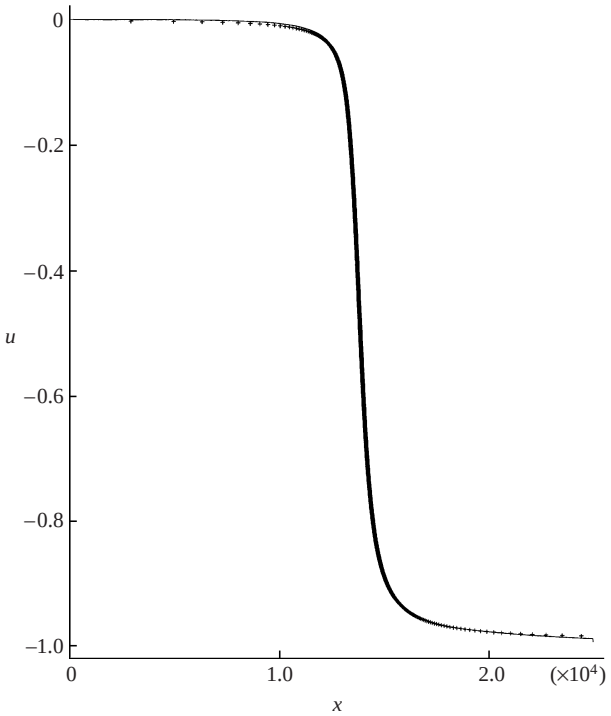

FIGURE 9. Comparison of the full numerical solution for $\tau = 2.55 \times 10^5$ (solid line) and the travelling wave solution (50) (+++).

where $\chi = x_4\tau_4^{-2/3}$. Letting $' = \mathrm{d}/\mathrm{d}\chi$, we find

$$p_3' + \gamma\rho_3\bar{u}_4^2 = 0, \quad -\tfrac{2}{3}\chi\rho_3' + (\rho_3\bar{u}_4)' = 0, \quad -\tfrac{2}{3}\chi p_3' + \gamma(p_3\bar{u}_4)' = 0, \tag{54}$$

with

$$p_3 \sim 1, \qquad \rho_3 \sim 1, \qquad \bar{u}_4 \sim 3\chi^{-2} \quad \text{as} \quad \chi \to -\infty,$$

and

$$\bar{u}_4 \to \infty \quad \text{as} \quad \chi \to +\infty. \tag{55}$$

This is a complicated two-point boundary value problem, but asymptotically there are solutions in which

$$\bar{u}_4 = O(\chi), \quad p_3 = O(\chi^{-\lambda}), \quad \rho_3 = O(\chi^{-\lambda-3}) \tag{56}$$

as $\chi \to +\infty$, with $\lambda = \sqrt{(4\gamma-1)/(\gamma-1)} - 1$, and the existence of these solutions has been confirmed by Hastings *et al.* (2001).

Supposing that (54), (55) are indeed capable of initiating such a motion we can rescale behind the piston by setting $x_4 = \epsilon^{-1/3}x_3$ (i.e. $x = \epsilon^{-3}x_3$), $\bar{u}_4 = \epsilon^{-1/3}u$ to derive (47)–(49) or (51)–(53) yet again. Now however we can apply the piston boundary condition

$$u = 1 \quad \text{on} \quad x_3 = \tau_4$$

and the matching condition

$$u \sim \text{const.}\, x_3/\tau_4 \quad \text{as} \quad x_3 \to 0;$$

this means that this transition region between the piston and its initial position can be

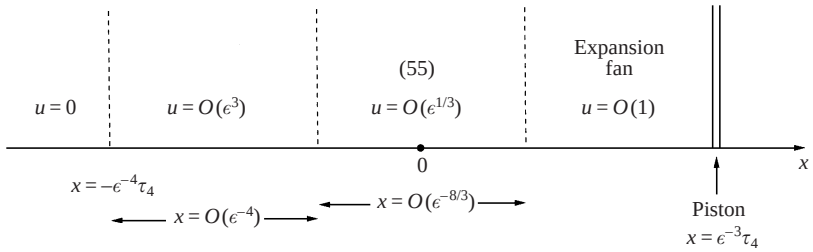

FIGURE 10. Solution of the expanding piston problem (§ 3.2.2): regions of the (x, τ)-plane.

described by a final similarity solution in which u, $p_3\tau_4^{\lambda/3}$ and $\rho_3\tau_4^{1+\lambda/3}$ are all functions of x_3/τ_4. Thus a Fanno 'expansion fan' describes most of the flow in $0 < x < \epsilon\tau$, and we expect this scenario to be uniformly valid for all $\tau > O(\epsilon^{-3})$ (see figure 10).

In summary, our analysis of waves of small Mach number ϵ has revealed that on a dimensional time scale L/a_0, where L is the Fanno length S_0/f, wall friction has negligible effect on acoustic waves. However, on time scales of $O(L/a_0\epsilon)$ to $O(L/a_0\epsilon^3)$, friction can build up appreciable pressures, leading to several nonlinear models that are awkward mathematically. Although in no small-ϵ flow have we been forced to study the full Fanno model (16)–(18), the analysis of § 3.2.1 provides strong motivation for a more general study of travelling compressive waves, which we expect to travel at a speed which is γ times the piston speed. The results of § 4 will confirm this, but also some unexpected properties of the waves will be revealed which even admit the possibility of travelling waves of expansion.

4. Travelling waves

We consider a wave of permanent form propagating with dimensional velocity V_0 into a stationary gas in which the sound speed is a_0 with velocity u_0 far behind the wave. Non-dimensionalizing as before and setting $V_0/u_0 = V$ and $x - Vt = \xi$ in equations (16)–(18) we find that

$$\rho(V - u) = V, \tag{57}$$

$$p(\gamma u - V) + \frac{u}{M_0^2} - (\gamma - 1)\frac{Vu^2}{2} = 0, \tag{58}$$

and

$$\frac{\mathrm{d}u}{\mathrm{d}\xi} = \frac{2\gamma u^2(\gamma u - V)^2}{(\gamma + 1)(u - V)(K - (\gamma u - V)^2)}, \tag{59}$$

where

$$K = \frac{2\gamma}{(\gamma + 1)M_0^2} - \frac{\gamma - 1}{\gamma + 1}V^2, \quad M_0 = \frac{u_0}{a_0}$$

and we have assumed that ahead of the wave $u \to 0$, $p \to 0$ and $\rho \to 1$.

We can study both compression and expansion waves by assuming $V > 0$ if we consider the boundary conditions

$$u \to 1 \quad \text{as} \quad \xi \to -\infty, \; u \to 0 \quad \text{as} \quad \xi \to +\infty \quad \text{for compression} \tag{60}$$

and

$$u \to 1 \quad \text{as} \quad \xi \to +\infty, \; u \to 0 \quad \text{as} \quad \xi \to -\infty \quad \text{for expansion.} \tag{61}$$

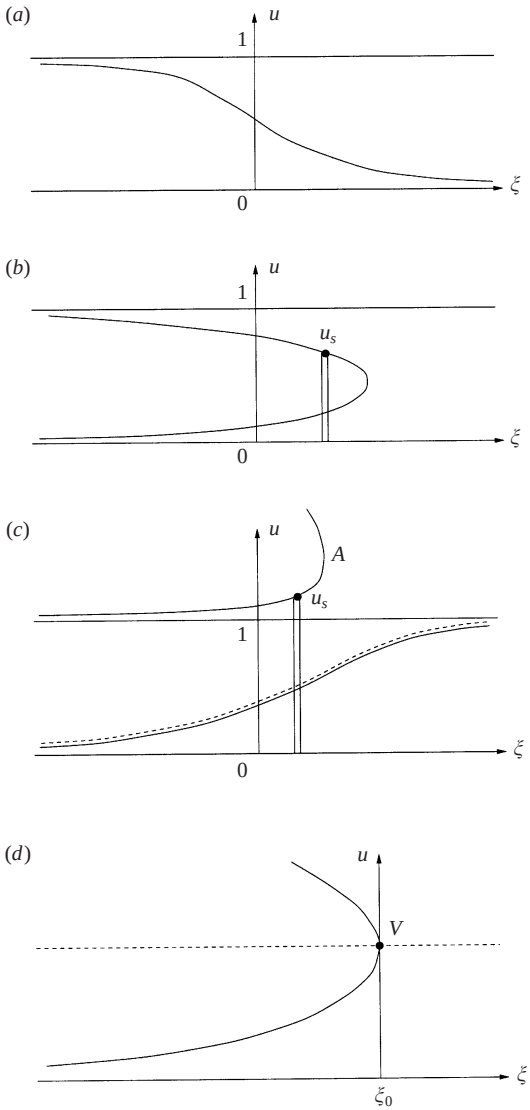

FIGURE 11. Travelling wave solutions: (*a*) $M_w < 1$, $V = \gamma$; (*b*) $1 < M_w < \sqrt{2\gamma/(\gamma-1)}$, $V = \gamma$; (*c*) $\sqrt{2\gamma/(\gamma-1)} < M_w$, $V = \gamma$; (*d*) $M_0 = \sqrt{2\gamma/[(\gamma-1)V^2]}$.

Since $u \to 1$ as $|\xi| \to \infty$ in both cases we must take $V = \gamma$ and we can then see that there are three possible regimes. It is convenient to classify them according to the value of the Mach number of the wave defined as $M_w = \gamma M_0 = V_0/a_0$.

(i) When $M_w < 1$, a continuous compression wave is possible, whose small-amplitude limit is, of course, the case considered in § 3.2.1 and this is shown in figure 10(*a*). The Mach number u/a is below unity throughout this wave.

(ii) For $1 < M_w < \sqrt{2\gamma/(\gamma-1)}$, it is still possible to find a steady travelling wave of compression but it is now necessary to introduce a shock moving with speed γ as shown in figure 11(*b*). Two of the Rankine–Hugoniot shock relations will be satisfied automatically across this shock since the equations (57) and (58) conserve mass and

energy and then conservation of momentum determines u behind the shock as

$$u_s = \frac{2\gamma}{\gamma+1}\left(1 - \frac{1}{\gamma^2 M_0^2}\right).$$

(iii) For even larger values of $M_w > \sqrt{2\gamma/(\gamma-1)}$, a compressive wave can still be found but as shown in figure 11(*c*), the velocity will *increase* as the shock is approached from the downstream side.

In this case we can also see that it appears to be possible to have a continuous *expansion* wave satisfying (61) and indicated by the dotted curve in figure 11(*c*). However closer inspection shows that the dimensional pressure as used in the gas law becomes negative for $\sqrt{2/[\gamma(\gamma-1)M_0^2]} < u < 1$ and so this is not a realistic solution. Nonetheless, because $u = \gamma$ at the vertical tangent in figure 11(*c*), an expansion wave can exist in which a piston at A moves with speed γ and the gas moves with speed $u = 1$ at $\xi = -\infty$.

A special case arises when, and only when, $M_0 = \sqrt{2\gamma/(\gamma-1)V^2}$ or $M_w = \sqrt{2\gamma/(\gamma-1)}$. In this situation the $(\gamma U - V)^2$ factors in (59) cancel and there is no reason to take $V = \gamma$. We can also see from (59) that the pressure can remain finite as $u \to V/\gamma$ whereas for other values of M_w, p tends to infinity in this limit. Then equations (58) and (59) simplify to

$$p = \frac{(\gamma-1)uV}{2\gamma} \quad \text{and} \quad \frac{\mathrm{d}u}{\mathrm{d}\xi} = \frac{2\gamma u^2}{(\gamma+1)(V-u)}.$$

Although the solution cannot extend over the whole line $-\infty < \xi < \infty$, it is possible to fit an expansion wave behind a piston at $x = Vt$ as shown in figure 11(*d*). The dimensional speed of the piston and the wave must be $\sqrt{2\gamma/(\gamma-1)}a_0$ for this solution, which is probably unstable, to be possible.

5. Conclusion

We have presented a self-contained derivation of the Fanno model for fully developed compressible perfect gas flow in a straight tube, the principal effect of the turbulence being to exert wall drag via the boundary layers. Our analysis of flow at small Mach number has revealed that even in problems that would be uniformly described by acoustic theory in laminar inviscid flow, the wall friction, which typically modifies the laminar model by a factor of $O(10^{-3})$, can engender significant nonlinearity over long enough times and distances. Although our mathematical analysis is far from complete, it suggests that flows driven by an initial release of energy, such as a 'blip' in a transducer, are localized in a region of $O(t^{2/3})$ near the source for large times, whereas piston motion can ultimately produce compressive flows in which the gas moves appreciably in an expanding region between the piston and a precursor wave moving with speed γ times the piston velocity. Expansions behind a piston can also occur in which the structure is quite different from the usual simple wave flow.

The solution of the fully nonlinear Fanno model must be undertaken numerically except for travelling-wave solutions. These differ from classical inviscid shocks in that continuous compressive waves are possible, with speed γu_0 if the Mach number $\gamma u_0/a_0$ of the flow downstream of the wave relative to the wave is less than unity, but, for higher values of this Mach number, discontinuities are necessary in compressive travelling waves. Interestingly, there is only one type of travelling expansion

wave behind a constant-velocity piston and that occurs when the piston velocity is $\sqrt{2\gamma/(\gamma-1)}$ times the speed of sound in the undisturbed gas.

From the computational viewpoint, the evidence in Ozawa & Maeda (1988), Terenzi *et al.* (2000), Hague *et al.* (1992), suggests that it is difficult to discern general rules for the long-time propagation of waves obeying the Fanno model. However, the small-amplitude theory both admits a consistent synthesis of the different spatio-temporal asymptotic regions and is amenable to treatment by a Godunov-type algorithm when the time step is taken sufficiently small. The agreement between the numerical and analytic approaches gives us confidence that the asymptotic results can be used to check computations in cases where nonlinearity is important from the start.

We would like to thank Mr H. Bendafi of Jaguar Cars, whose MSc thesis started this investigation and Dr M. Jones for his many helpful comments.

REFERENCES

Falle, S. A. E. G. 1991 Self-similar sets. *Mon. Not. R. Astron. Soc.* **250**, 581–596.

European Study Group with Industry 1997 Final report. Maths Dept, University of Bath.

Garabedian, P. R. 1964 *Partial Differential Equations.* Wiley.

Hague, M. A., Richardson, S. M., Saville, G., Chamberlain, G. & Schirvil, L. 1992 Blowdown of pressure vessels II: Experimental validation of computer model and case studies. *Trans. Inst. Chem. Engrs* **70**, 10–17.

Hastings, S., McLeod, J. B. & Troy, W. 2001 Boundary-value problems in the Fanno model for turbulent compressible flow. *Proc. R. Soc. Edin.* (to appear).

Jones, T. V., Oldfield, M. L. G., Ainsworth, R. W. & Arts, T. 1993 Transient cascade testing. In *Advanced Methods for Cascade Testing, AGARDOGRAPH* 328 (ed. C. Hirsch), Chap. 5. AGARD NATO.

Knight, D. D. 1998 Inviscid compressible flow. In *The Handbook of Fluid Dynamics.* CRC.

Landau, L. D. & Lifschitz, E. M. 1959 *Fluid Mechanics.* Pergamon.

Liepmann, H. W. & Roshko, A. 1957 *Elements of Gas Dynamics.* Wiley.

Ozawa, S. & Maeda, T. 1988 Model experiment on reduction of micro-pressure wave radiated from tunnel exit. *Proc. Intl Symp. on Scale Modeling*, vol. 7, pp. 18–22. The Japan Society of Mechanical Engineers.

Shapiro, A. H. 1953 *The Dynamics and Thermodynamics of Compressible Fluid Flow*, vol. I. The Ronald Press Co. New York.

Terenzi, A., Mancini, N. & Podenzani, F. 2000 Transient compressible flow in pipelines: a Godunov-type solver for Navier-Stokes equations. Preprint.

Wright, D. & White, K. P. Jr 1974 Dynamics of pneumatic-tube vehicles. *Trans. ASME* G: **96**, 229–235.